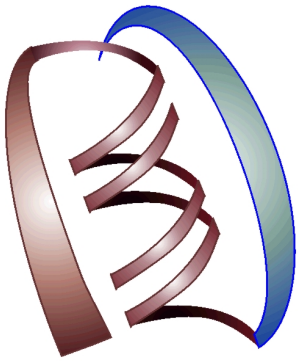

BIOMEDICAL
ENGINEERING

Carnegie Mellon University

2016 Biomedical Engineering Summer Undergraduate Research Symposium

July 27, 2016

Scott Hall 4N200

9:00 AM to 1:00 PM

Biomedical Engineering at Carnegie Mellon University
Biomedical engineering education at Carnegie Mellon reflects the belief that a top biomedical engineer must be deeply trained in both a traditional engineering practice and biomedical sciences. The unique additional major program leverages extensive collaborations with sister departments in the College of Engineering and with major medical institutions in Pittsburgh. This collaborative approach, combined with a rigorous engineering education, confers unique depth and breadth to the education of Biomedical Engineering graduates.

Biomedical Engineering Summer Undergraduate Research Program (BME SURP)
This program allows students to spend a ten-week period on a project that combines translational research and clinical exposure at a local medical center. Hundreds of students have participated in BME-SURP since its introduction in 1980. The experience have played a major role in helping students choose their career paths and obtain positions in industrial or academia. This program is supported by grants from the CMU College of Engineering, Merck & Co., Inc., and the CMU University Research Office (URO).

Carnegie Heart Program
The Carnegie Heart Program is a collaborative effort between the Biomedical Engineering Department at Carnegie Mellon University and the Allegheny Health Network. The purpose of this program is to develop biomedical engineers who can apply their education toward new technologies for clinical cardiovascular medicine. In addition to students' experience in a laboratory setting, students will shadow cardiovascular clinicians at Allegheny General Hospital one day every two weeks. This program is supported through a grant from the American Heart Association.

Presentation Schedule

9:00 AM	Samantha Shoemaker (Carnegie Heart)
9:15 AM	Gayatri Paranjape (BME SURP/URO)
9:30 AM	Edward Healy (Carnegie Heart)
9:45 AM	Mary Jin (Carnegie Heart)
10:00 AM	Alexandra Vendetti (Carnegie Heart)
10:15 AM	Molly Kaissar (BME SURP)
10:30 AM	**BREAK**
10:45 AM	Michelle Wu (BME SURP)
11:00 AM	Julia Napolitano (BME SURP)
11:15 AM	Yushuan Peng (BME SURP)
11:30 AM	Diva Bramharouthu (BME SURP/ URO)
11:45 AM	Yuanyuan Fu (Carnegie Heart)
12:00 PM	**Lunch and Cake**

Note: Nin Rebecca Kang (Carnegie Heart), and Aakash Parekh (BME SURP/URO) presented earlier in a separate presentation

Quantification and Modeling of Clot Formation on Artificial Lung Fibers

Samantha Shoemaker, Keith Cook, Wei-Tao Wu
Carnegie Mellon University

Introduction: Extracorporeal membrane oxygenation and artificial lung technology are currently unable to function regularly as long term support for chronic lung disease patients. One of the primary reasons for failure of oxygenating devices is clot formation. Relevant design variables whose impact on clot formation we do not yet understand are fiber bundle shape, fiber bundle packing density, and gas exchange membrane material. While computational fluid dynamics gives a macroscale overview of flow, a more detailed and nuanced model of clot formation is needed for improving device performance. In order to validate and use an existing model, material-dependent constants need to be found by comparing quantitative and qualitative experimental results to the simulated thrombus. The methodology of both the data analysis and the experiments themselves is necessary.

Materials and Methods: Fibers were weighed then immersed in recalcified and heparinized sheep's blood and incubated on an orbital shaker for 4 hours. They were removed and rinsed five times with PBS before being immersed in 2% glutaraldehyde for 24 hours. To prepare for imaging, the fibers were rinsed with PBS three times and once with deionized water. They were then imaged at 20x magnification with a 488 nm laser every 15 μm in the vertical direction to create a stack of images. The stack was imported into ImageJ and a binary threshold, where clot is black, was applied along with a despeckle filter. BoneJ[1] was used to determine the volume of the clot by assuming a depth of each clotted pixel to be 15 μm, the distance between images in a stack.
A basic setup of a syringe pump, tubing, a stopcock, and a tubing connector was used as a trial attempt for generating clot formation data. The single fiber was held between the connector and the tubing, and 60 mL of recalcified sheep blood was run at 5 mL/min through the setup.

Results and Discussion: Initially, entire stacks of fiber layers were imaged, but the fibers interfered with a clear view of the clot throughout the layers. This method also failed when the thrombus was too thick and fluorescence was detected only on the top sections. The successful trial used a single fiber layer with minimal clot formation.
The mass difference of the successfully imaged fiber layer before and after clot was 5.4 mg. Using a threshold in ImageJ of 0 to 1, the volume of clot was found to be 4.14 mm^3. Assuming a clot density of 1080 kg/m^3, this clot weighs 4.47 mg, which has an error of 17% from the experimental clot mass. A threshold of 0 to 2 resulted in a mass of 2.86 mg, an error of 47%, thus this method is sensitive to user-set parameters. Figure 1 shows an original and processed image with the threshold of 0 to 1.
With the syringe pump setup, the fiber showed moderate clot formation on the side of indirect flow after 12 minutes. Results may be confounded by the non-fiber blood-contacting surfaces and the stretching of the fiber.

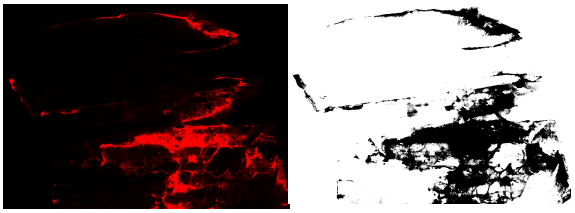

Figure 1. A preprocessed image of the fiber layer (left) and the thresholded and despeckled image (right). The processing preserves the information of the original image.

Conclusions: Fixing fibers in glutaraldehyde and imaging the layer to find the thrombus volume is a potential technique to determine whether the model's material constants are accurate. This method, however, only works for a single layer of fibers with minimal to moderate clot (i.e. where the fibers themselves are still visible beneath the clot). Different thresholds and amounts of clot need to be used and imaged in order to further determine the optimal parameters and situations for this methodology.
The experimental setup for creating clot on fibers in flow needs to be modified with alternative components to reduce the surface area of the components and the deformation of the fiber.

Acknowledgements: This research was supported by the American Heart Association.

References: Doube M, Kłosowski MM, Arganda-Carreras I, Cordeliéres F, Dougherty RP, Jackson J, Schmid B, Hutchinson JR, Shefelbine SJ. (2010) BoneJ: free and extensible bone image analysis in ImageJ. Bone 47:1076-9. doi: 10.1016/j.bone.2010.08.023. Version 1.4.1.

Nitric Oxide Generating Surface to Reduce Clot Formation in Artificial Lungs

Gayatri Paranjape, Angela Lai
Carnegie Mellon University

Introduction

A staggering one in six US deaths is caused by lung disease, because the needed treatment of a lung transplant isn't widely available to patients. Therefore, patients temporarily use an artificial lung before receiving a lung transplant. ECMO, or extracorporeal membrane oxygenator, is the current bridge to transplantation. However, it only lasts a few weeks due to its large circuit, which creates significant clotting, and ultimately leads to multiple organ failure. Thus, improvements to artificial lungs are necessary to ensure patients can survive.

The largest site of blood clot in artificial lungs is the fiber bundle, which is the site of gas exchange. Nitric oxide, or NO, can be used to prevent clot formation. NO acts by biding to guanylyl cyclase, guanylyl cyclase hydrolyzes GTP to cGMP, and cGMP binds to protein receptors of platelets. Thus, platelets cannot bind to their receptors and form a clot.

This study aims to test how effective a PDMS coating with Cu particles that generates NO is at preventing clot formation in the fiber bundles of an artificial lung.

Materials and Methods

In order to determine how effectively NO prevented clot formation, an in vivo sheep experiment was ultimately conducted, using devices with copper impregnated fibers that generate the NO. Cu is a catalyst in a reaction that decomposes an RSNO molecule, resulting in the release of NO. In the case of this study, the RSNO used was SNAP, and it was injected into the sheep.

Before the in vivo testing, devices were prepared for use. Water and gas leak testing was conducted. Essentially, the device was filled with either water or gas, and observed to see whether there were any leaks. If there were, the leaks were patched. The leak testing was done to ensure that when the device was used in an experiment with blood going through it, all of the blood would go into the fibers so gas exchange would occur. Water and gas resistance testing was conducted as well, by pumping either water or air through the device, and measuring the resistance. This determined whether any of the fibers in the fiber bundle were plugged, and therefore if gas exchange would occur effectively in the device.

Once the devices were ready, a benchtop experiment was conducted. Blood was pumped through a circuit with the devices, to see how well they oxygenated the blood and removed carbon dioxide.

Finally, two 72 hour in vivo experiments with sheep were conducted. Using ECMO, a control device and a copper device were connected to the sheep, so that the two could be compared, in terms of how long each lasted, and how well each performed gas exchange. The control device used fibers that are currently commercially available, whereas the copper device used the biomaterial which will form NO. During this experiment, measurements were taken to monitor the health of the sheep, as well as to see how well the devices were working. The resistance of the device was measured, and was replaced when it had increased by 200%. This meant that the device had failed.

Results and Discussion:

The gas exchange experiment showed that a flow rate of 300ml/min for the blood was best for oxygen exchange. At this flow rate, an average of 79.33 ml of oxygen were exchanged per minute. For a flow rate of 150 ml/min, 46.99 ml of oxygen were exchanged per minute. The flow rates of 450 and 600 ml/min had an average of 68.98 and 72.19 ml of oxygen exchanged per minute, respectively.

Thus, a flow rate of 300ml/min was chosen for the in vivo sheep experiments. During this experiment, the control device failed after 27 hours, and the copper device functioned for the duration of the experiment, which was 72 hours.

Conclusion

The implication of these results is that since the copper device fails later than the control device, the biomaterial used which reacts to form NO seems to prevent clot formation. In the future, more in vivo sheep experiments should be conducted to further verify these results. Longer term studies, such as for two months, should be conducted as well, in order to determine how effective these devices can be when used as a bridge to transplant in patients.

A Look at the Standard Electrocardiogram: Is it Possible to Measure the His Signal Noninvasively?

Edward W. Healy, Emerson H. Liu, MD.
Carnegie Mellon University, Allegheny Health Network.

Introduction: The electrocardiogram (ECG) has been used to record the electrical impulses of the heart for over a century; however, the system has remained relatively unchanged. While electrical signals pertaining to myocardial depolarization are typically on the scale of millivolts (mV), those pertaining to activation of the normal conduction system, such as the His-Purkinje system, are on the scale of microvolts (μV). Since the His signal is on such a small scale, current ECG systems do not have the ability take its measurement. Current measurement of the His signal must be done invasively, most often during an electrophysiologic (EP) study.
The His signal is a great tool to determine the site and severity of transient heart block. For this reason, it would be advantageous to design an ECG that has the ability to measure the conduction of the His-Purkinje system to reduce the need for invasive diagnostic procedures.

Materials and Methods: In this study, His points were taken from patients undergoing EP studies for various reasons, most often to treat arrhythmias through heart ablation surgery. During these surgeries, the BioSense CARTO 3 system was used. This system is composed of an advanced imaging technology that uses electromagnetic localization catheters to create real-time three-dimensional (3D) maps of a patient's cardiac structure. Through the use of this technology, it was possible to take an intracardiac measurement of the His signal directly from the patient's His-Purkinje system using one of the localization catheters. Next, this system was used to project the mapped location of the His-Purkinje system onto the patient's body surface. This projection was made in the hopes that placing a lead directly above the His-Purkinje system would provide the highest chance of obtaining a His signal from a point taken on the body surface. From that point, two body surface readings of the patient's ECG signal were taken first using a unipolar localization catheter and second using a bipolar lead from a standard ECG system. These two measurements were taken in order to make a comparison between the use of unipolar and bipolar leads in the interest of creating the optimal ECG system. After these measurements were taken, MATLAB was used to process these signal measurements using various techniques such as signal averaging and signal summation. These techniques were applied to both raw and moving averaged signals to determine the need for different signal processing steps.

Results and Discussion: Throughout this study, data was taken from 8 patients most of whom were elderly and overweight. In the case of all patients, a His signal could not be identified on the body surface using neither a unipolar localization catheter nor a bipolar lead from a standard ECG system. For this reason, different methods of signal processing were applied to the intracardiac His signals in the expectation that these methods would apply to the body surface recordings if the His signal was eventually located. It seemed that signal averaging was superior to signal summation. Both methods produced the same waveform; however, signal averaging allowed for the analysis of the actual characteristics of the signal itself, such as amplitude of the signal, while signal summation provided the same waveform but greatly increased the amplitude. Along with this, it seemed that applying a moving average to the raw signal was not necessary, except in the interest of smoothing the waveform.

Conclusions: Since most of the patients were elderly and overweight (only one patient was below 60 years old and healthy with respect to weight), it may be concluded that the His signal cannot be measured from the body surface using current technology. With age, the His-Purkinje fibers do not conduct as strong of a signal in comparison to younger patients. Along with this, overweight patients have a larger chest size. This means that the His signal would have a larger pathway to travel than in patients who have maintained a healthier weight. From the data taken from applying techniques to the intracardiac signals, the ideal setup for a new ECG device would include a moving average on the raw signal along with applying a signal average to past beats in order to achieve isolation of the His signal. Signal averaging of previous beats would be required since it would be expected that the His signal would be much smaller on the body surface than on intracardiac readings.

Acknowledgements: The author would like to thank Dr. Emerson Liu and Dr. Keith Cook for their guidance throughout this project. The author would also like to thank the American Heart Association for providing funds to make this project possible.

Subcutaneous and Cutaneous Blood Flow Imaging Using Forward Looking Infrared System

Mary Jin, Chao Liu, Srinivasa Narasimhan
Carnegie Mellon University

Introduction: Abnormality in subcutaneous and cutaneous blood flow is indicative of many diseases and injuries. The goal is to observe subcutaneous and cutaneous blood flow using a non-invasive, accurate, and quantitative method. The Forward Looking Infrared imaging (FLIR) can measure small temperature difference cased by abnormal blood flow such as that due to melanoma. Quantitative analysis of FLIR imaging can help surgeons determine range of operation and recovery rate when removing the melanoma.

Materials and Methods: The subjects of this study were melanoma patients who have already been through biopsy. A FLIR T640 camera was set up in the Operating Room on a tripod and was calibrated. Before and after each surgery, the surgeon applied wet cloth to region of interest (ROI) for 30 seconds to cool the skin. A 2-minute long video was recorded as the skin recovered to room temperature. After the melanoma was removed and skin was stapled, several 1-minute long videos were recorded with 5-10 minute interval in between. All the videos first went through motion compensation. Over 500 features were found from the video utilizing FAST (features from accelerated segment test) detector and were then matched using HOG (histogram of oriented gradient) descriptor. Once the motion caused by breathing and camera movement was compensated, the ROI is selected manually. As the gray scale of each pixel changes throughout the video, the variance and range were calculated for each pixel.

Results and Discussion:
Melanoma detection: After the cooling cloth is applied, the lesion's temperature rises faster than healthy tissue. This rapid change of temperature can be seen on Figure 3, where the bright spot indicates greater variance. The location of the bright spot corresponds to the location seen in biopsy. For the video taken after surgery, the skin is not cooled uniformly. The variance image is not representative of blood flow and could not be used as reference.
Surgery recovery: After the melanoma is removed and skin is stapled, the blood flow slowly restores. The dark area in Figure 1 suggests lower temperature compared to surrounding tissue. The same area experiences a temperature increase, as seen in the gray blotch in Figure 2. The surrounding tissue has almost no temperature change, therefore remains dark.

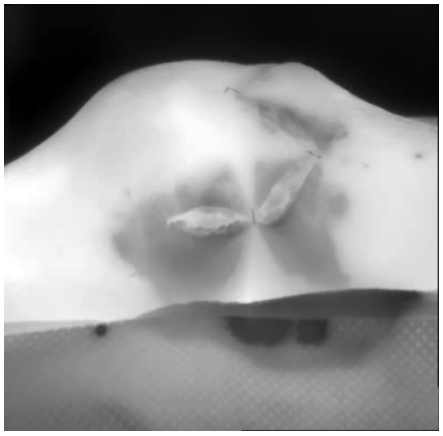

Figure 1: Infrared image of patient's left knee. This is the first frame of the video shown in Figure 2.

Figure 2: Variance of temperature across 1 minute. Video taken 15 minute after skin was stapled. Gray blotch indicates temperature increasing.

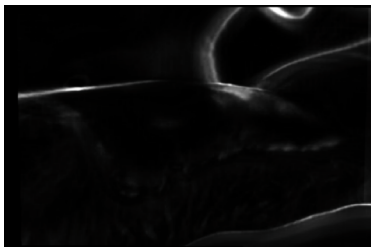

Figure 3: Variance of temperature across 2 minutes. Video is taken before surgery. Melanoma is shown as bright spot by elbow, located on patient's left arm.

Conclusions: With the aid of motion compensation, FLIR imaging is a promising non-invasive procedure to observe changes in subcutaneous and cutaneous blood flow. The goal is to introduce an automated imaging tool to help surgeons determine the range of surgery and predict the rate of recovery after the surgery. With more recordings being done under standardized procedure in the future, a classifier will be built to assist the diagnosis.

Acknowledgements: This research is supported by the American Heart Association. We would like to thank Dr.Howard Edington who provided expertise and gave permission to all required equipment and materials.

Measuring the Effect of Fibroblast Co-Culture on Compaction of Engineered Human Cardiac Muscle

Alexandra Vendetti
Carnegie Mellon University

Introduction: The purpose of this research is to develop a 3D cardiac muscle tissue by co-culturing human embryonic stem cell-derived cardiomyocytes (CMs) with cardiac fibroblasts. Previously, contractile 3D cardiac muscle micro-tissues were engineered by casting collagen I (Col I) gels embedded with CMs, which had an initial diameter of ~ 3mm. This is problematic because there is a diffusion limit since cultured tissues do not have a blood vessel network, so cells need to be within 100um of media for nutrient, oxygen and waste exchange. CMs alone have limited ability to remodel and condense the initial volume of surrounding Col I matrix. These engineered tissues were co-cultured with various percentages of fibroblasts, cells that specialize in making and remodeling surrounding extracellular matrix, in order to engineer more cell-dense, synchronously beating cardiac micro-tissues with less 'dead-space' due to diffusion limits. Engineered tissues with 0%, 3%, 10%, and 20% fibroblasts were imaged daily to measure the total construct area to track tissue compaction over the course of 10-14 days. After two weeks of culturing, the micro-tissues undergo pharmacological testing and electrical stimulation to determine the excitation threshold and examine how beat frequency and force generation are affected by drug treatment. The eventual applications are to create an in vitro model of human heart muscle for drug discovery and toxicity screening and for personalized treatment using patient-specific induced pluripotent stem cells.

Materials and Methods: In order to create the micro-tissues, an ABS mold was 3D printed from a CAD model and polydimethylsiloxane (PDMS) was poured into the plastic mold and left to cure to create wells for culturing 3D cardiac micro-tissues. Dog-bone shaped silicone inserts were folded into a U conformation and placed into small slits in the base of the PDMS wells. In this way, either end of the 'U' served as an attachment point for the cardiac micro-tissues and allowed for easy removal of beating constructs from the wells for contractility testing. Insert thickness was measured using a profilometer to calculate force generated by the beating tissues. HUES9 derived CMs were cast with either 0%, 3%, 10% or 20% ventricular cardiac fibroblasts. Tissues were imaged using a stereomicroscope and images were analyzed to track compaction area using ImageJ. After 10-14 days the tissues were compacted enough for stimulation.

Results and Discussion: As the fibroblast concentration used increased, the compaction of the micro-tissue increased as seen with the trends in Figure 1. Tissues with fibroblasts compacted to a smaller area than tissues with 0% fibroblasts, which did not form mature tissues. Overall tissue compaction was compared for 0%, 10%, and 20% fibroblast tissues. Tissues with 20% fibroblasts compacted significantly more than tissues with 0% or 10% fibroblasts by day 10. Additionally, 10% fibroblasts tissues also compacted significantly more than tissues with 0% fibroblasts by day 10. However, 36% of the tissues with 20% fibroblasts broke by day 10 of culture due to much less uniform compaction by the fibroblasts. This can be compared to the 15% of tissues with 10% fibroblast that broke by day 10. The tissues with 10% fibroblasts appeared to compact more uniformly and were able to be maintained in culture at least 14 days, where the tissues were also demonstrated to be significantly stronger.

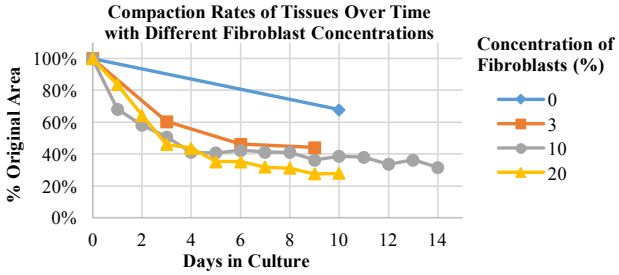

Figure 1: The compaction rates of the cardiac muscle tissues over time with four different fibroblast concentrations

Conclusion: Since the micro-tissues with 0% fibroblast were not significantly remodeled, a certain percentage of fibroblasts are needed in the gel to form a more compact, mature tissue. As the fibroblast concentration increased, the rate of tissue compaction increased. Tissues with 20% fibroblasts compacted more but less consistently and risked the micro-tissues breaking before the contractility assay. Tissues with 10% fibroblasts compacted at slower rates than with 20% fibroblasts but compaction appeared more uniform, and constructs were able to be maintained in culture for longer periods of time. It was determined that the fibroblasts have the best contractions after culturing them for at least 14 days. Since the tissues with 20% fibroblasts break after day 10, it is best to use tissues with 10% fibroblasts.

Acknowledgements: Thank you to Allegheny Health Network for providing funding for the Carnegie Heart Program. Thank you to Professor Feinberg for providing resources and allowing me work in his lab and to Rebecca Duffy for guiding me through the summer project and running experiments.

The Use of Hydrophobic Light Activated Adhesive (HLAA) for the Adhesion of a Torsional Ventricular Assist Device (tVAD)

Molly Kaissar, Elaine Soohoo, Dennis Trumble

Introduction: One of the present limitations in the development of the torsional ventricular assist device (tVAD) is finding a suitable method of long-term device fixation. The tVAD attaches to the apex of the heart and provides cardiac assist by rotating the ventricles, which helps to unload the ventricles and reduce shear stresses in the myocardial walls.[4] Previously, active suction has been used as a method of short-term device fixation, but in order to avoid damaging the myocardial tissue during longer-term usage, we propose a biphasic attachment scheme that would utilize a bioadhesive for an initial attachment to the heart and allow for scar tissue to form and develop into our primary method of attachment. In selecting an appropriate bioadhesive for this, there are various factors that must be addressed. The details we have opted to focus on include (i) the lifespan of the bioadhesive, (ii) its ability to withstand shear stress, and (iii) the types of surfaces it can adhere to.

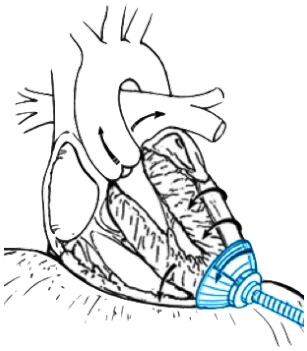

Figure 1. Artist's rendering of the tVAD.

Materials and Methods: To select adhesives that would support the tVAD, we studied papers of common adhesives with these criteria in mind. In order to work with the tVAD, the bioadhesives must bond for long enough to secure the device until tissue ingrowth occurs, be able to withstand shear stresses of the device, and be able to adhere to wet, smooth tissue at average body temperature in order to glue the device to the epicardium. Each potential adhesive was eliminated if they did not have evidence proving the device could meet these requirements. Materials considered for this project were DOPA, alginate-based glues, cyanoacrylate, polyglycerol sebacate (PGS), polydopamine, and hydrophobic light activated adhesive (HLAA).[1]

Results and Discussion: Based on these criteria, we have selected hydrophobic light activated adhesive (HLAA) as our desired adhesive. Tested at the Boston Children's Hospital, Brigham and Women's Hospital, and Massachusetts Institute of Technology, HLAA is a bioadhesive designed with hearts in mind and is a promising solution to our fixation dilemma. The adhesive is composed of a prepolymer of polyglycerol sebacate acrylate (PGSA) that is exposed to UV light, transforming the fluid into a flexible solid in seconds.[1-3] In the article by Lang et al., the adhesive was subject to various tests that proved it could be used for medical devices, similar to the tVAD, as it could adhere to patches of epicardial tissue for long periods of time and withstand high levels of stress.[1] It is also ideal for surgery due to its short curing time.[1-3]

Conclusions: To adhere the tVAD to the apex of the heart, we propose using HLAA to secure the epicardium to a "glove" covering the actuators of the device, which will serve as an interface between the heart and the device. Additionally, we would like to promote scar tissue formation to replace the bioadhesive over time, either through wound healing signaling cues or by lightly abrading the epicardial surface. To move forward with this research, we need access to HLAA or its components, a source of UV light for curing, and cardiac tissue for testing. Over the next few months, we plan to see if HLAA will adhere to cardiac tissue, create a glove for the apex of the heart, and eventually test the adhesive and glove with the tVAD.

Acknowledgements: I would like to thank the Biomedical Engineering Summer Undergraduate Research Program (BME-SURP) for supporting this project.

References:

1. Lang, N., Pereira, M. J., Lee, Y., Friehs, I., Vasilyev, N. V., Feins, E. N., ... & Padera, R. (2014). A blood-resistant surgical glue for minimally invasive repair of vessels and heart defects. *Science translational medicine*, *6*(218), 218ra6-218ra6.
2. Nguyen, K. T., & West, J. L. (2002). Photopolymerizable hydrogels for tissue engineering applications. *Biomaterials*, *23*(22), 4307-4314.
3. Nijst, C. L., Bruggeman, J. P., Karp, J. M., Ferreira, L., Zumbuehl, A., Bettinger, C. J., & Langer, R. (2007). Synthesis and characterization of photocurable elastomers from poly (glycerol-co-sebacate).*Biomacromolecules*, *8*(10), 3067-3073.
4. Trumble, D. R., McGregor, W. E., Kerckhoffs, R. C., & Waldman, L. K. (2011). Cardiac assist with a twist: apical torsion as a means to improve failing heart function. *Journal of biomechanical engineering*, *133*(10), 101003.

Optimization of Operating Points for Non-Invasive Cardiac Imaging Modalities under Clinical Conditions

Michelle Wu, Mark Doyle Ph.D, Geetha Rayarao, Robert Biederman MD.
Carnegie Mellon University, Allegheny General Hospital

Introduction: In the absence of strict criteria, interpretation of non-invasive cardiac images, such as CTA and SPECT, relies on physician training and lab culture. In part, that lab culture includes an element of interaction with the cath lab, and in particular a tolerance for the number of false positive patients. All modalities can be characterized by a receiver operator characteristic (ROC) curve, with the operating point on that curve representing a compromise between sensitivity and specificity (sens/spec). We note that as sensitivity increases, specificity necessarily decreases, resulting in a linearly increasing rate of false positive patients. We sought to examine the literature to ascertain what the community consensus was on operating point and whether there were differences between modalities.

Materials and Methods: Studies published after 2009 that used non-invasive cardiac imaging to determine coronary artery disease (CAD) were selected. Studies were then categorized as describing either 1) routine clinical use or 2) comparison of modalities. For clinical studies, the sens/spec values are not given so they were evaluated based on the CAD pretest likelihood and by using the number of people with disease found in the cath lab or the number of people revascularized as the true positive. For modality studies, sens/spec values were given and were extracted. Microsoft Excel was used to calculate the sens/spec and to plot the operating points. A student t-test was used to find p values.

Results and Discussion: For clinical studies, average sens/spec values were 24$\pm$23% and 92$\pm$7% for SPECT, 31$\pm$22% and 92$\pm$6% for CTA, and 17% and 93% for PET. For modality comparison studies, sens/spec values were 70$\pm$7% and 73$\pm$9% for SPECT, 88$\pm$10% and 90$\pm$1% for PET, 95$\pm$5% and 81$\pm$14% for CTA and 75$\pm$27% and 88$\pm$9% for MRI. The sensitivity for SPECT and CTA clinical studies were lower than modality studies ($p=.07$ and $p<.001$ respectively). The high sens/spec values of modality comparison studies show that the imaging modality performance is not in question. For a certain modality, the receiver operator characteristics are defined by the fundamental properties of the modality, but the operating point is defined by the image interpreter. The operating points could be closer to the optimal point, the point on the curve closest to 100% sensitivity and specificity, but clinical conditions force them to have a lower sensitivity. Meanwhile, specificity is high because a specificity below 75% would lead to too many healthy people being sent to the cath lab.

Conclusions: This study looks at where the optimal sensitivities and specificities of non-invasive cardiac imaging modalities lie on an ROC curve under clinical conditions. It is confirmed that for clinical studies, sensitivity is low and specificity is high due to clinical constraints. In addition, both clinical and modality comparison studies all had a fixed specificity above 75%. Future work would include finding more clinical studies to see if this trend applies and to continue tracking cath lab numbers to see if this trend continues.

Developing Engineering Controls for a Robotic System for Continuous Urine Collection

Julia Eve Napolitano
Departments of Biomedical Engineering, Chemical Engineering

Introduction

There are 5 million patient admissions to the Intensive Care Unit (ICU) in the United States each year[1], and Acute Kidney Injury (AKI) can affect up to 60% of patients over their stay in the ICU[2]. Urinary biomarkers can be used to improve the recognition and understanding of AKI on a molecular level, but give only a "snapshot" of a dynamic process. To truly understand and prevent possible threats to the kidney, a more reliable method of collecting multiple samples over time is necessary. The Rosenbloom Laboratory is developing a low-cost, robotic device to collect time-stamped urine samples non-invasively and autonomously. The device operates at a patient's bedside, pumping 85 uL of urine per hour through microtubing to a Y-connector (Figure 1.b.), where fluorocarbon spacers are injected between samples. In order to ensure that the device is operating safely, several engineering controls were developed this summer to prevent sample backflow, including a conductance sensor and a pinch valve (Figure 1.a.c.).

Materials and Methods

To manufacture the conductance sensor and valve, a form of additive manufacturing called stereolithography (SLA) was used. The sensor and valve were designed using SolidWorks and uploaded to Asiga Composer software. The 3D printer used was Asiga PICO2. The printer resins were composed of poly(ethylene glycol) diacrylate (PEGDA) as the monomer, Irgacure® as the photoinitiator, and either 0.6% Sudan I or 0.2% 2,5-Bis(5-tert-butyl-benzoxazol-2-yl)thiophene (BBT) as the absorber. The conductance sensor electrode is composed of MG Chemicals Silver Conductive Epoxy, using ethanol as a solvent. The normal concentration of sodium in the urine is >20 mM. To test conductivity, 12.5 mM to 200 mM sodium chloride solutions were prepared. The pinch valve utilizes a Power HD High-Speed Digital Micro Servo DSM44 motor.

Results and Discussion

The quality of the 3D printed sensor and valve were optimized by iteratively changing the settings, including slice thickness, exposure time, burn-in wait time, burn-in normal time, and base plate settings. The 0.6% Sudan I resin was rejected in favor of printing with the 0.2% BBT resin due to the fact that the latter printed higher-quality parts more time-efficiently.

It was determined that the optimal length of each electrode compartment and the distance between electrodes was 6 mm and 1.2 mm, respectively. The most effective ratio of epoxy to ethanol is 7 g epoxy/mL ethanol. The salt concentration and voltage detected follow a positive linear trend. Using 12.5 uM and 200 uM NaCl, 0.115 V and 0.846 V were detected (background: 0.100 V), respectively.

It was determined that the torque required to maneuver the valve slider was 0.31 kg·cm, and that the RC Servo had the capacity to properly pinch shut the microtubing in the valve (Figure 1.a.).

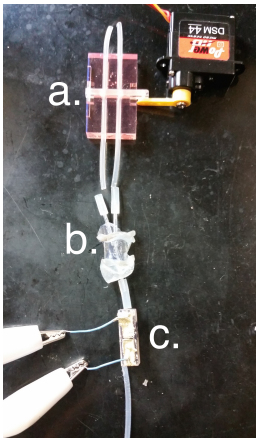

Figure 1. a. Pinch valve and Servomotor
b. Y-connector
c. Conductance sensor

Conclusion

The conductance sensor and pinch valve are feasible engineering controls to ensure the patient safety of the device. The conductance sensor is sensitive enough to read voltage at a minimum of 12.5 mM NaCl. The pinch valve is effective at pinching the microtubing closed to ensure no backflow into the sterile patient urinary collection system. Future studies should be performed to improve conductivity of the sensor and optimize mass production of device components.

Acknowledgements

The author would like to thank Dr. Alan Rosenbloom for his continued support regarding this project.

References

1. Utilization of Intensive Care Services, 2011. Agency for Healthcare Research and Quality (AHRQ). http://www.hcup-us.ahrq.gov/reports/statbriefs/sb185- Hospital-Intensive- Care-Units- 2011.pdf
2. Bellomo R, Kellum JA, Ronco C. Acute Kidney Injury. Lancet 2012; 380:756-766.

Comparison of Porcine Plasma and PBS in an In-Vitro Model of Sonoreperfusion

Yushuan Peng, Francois Yu, Xucai Chen, John Pacella
Carnegie Mellon University, University of Pittsburgh: Center for Ultrasound Molecular Imaging and Therapeutics

Introduction

Cardiovascular disease accounts for one in three deaths in the United States (Go et al. 2013). The most common current treatments for acute myocardial infarction (AMI) are thrombolytics, such as tissue plasminogen activator (tPA) and percutaneous coronary intervention, otherwise known as stenting. While those treatments lead to successful reperfusion of the artery, the microvasculature downstream can become obstructed by micro-embolization of the original obstruction, leading to poor functional recovery of thee patient (Ito et al. 1996). Use of thrombolytics can cause bleeding complications, also leading to poor recovery (Jong et al. 2001). Sonoreperfusion therapy seeks to reperfuse the microvasculature using ultrasound and microbubbles (MB). This study sought to compare the effects of sonoreperfusion with thrombolytics in phosphate buffered saline (PBS) and porcine plasma.

Materials and Methods

In this *in vitro* model of microvascular obstruction, PBS or porcine plasma was passed through tubing and casted rubber containing a 40 μm pore mesh. The mesh was occluded with prepared venous microthrombi, raising the upstream pressure to 40±5 mmHg. Therapeutic ultrasound was delivered with stable cavitation (where the MB oscillates at a constant rate), inertial cavitation (where the MB burst), or no ultrasound with and without tPA for twenty minutes in both porcine plasma and PBS for at least three trials for each combination. The resulting pressure drop of the experimental parameters were compared for both porcine plasma and PBS to determine the efficacy of each treatment regime.

Results and Discussion

It was discovered that tPA in porcine plasma caused complete reperfusion in the system whereas tPA in PBS only caused a slight drop in pressure after the treatment period (see Figure 1). Results presented later will show that the fastest reperfusion was caused by US in the inertial cavitation regime with tPA in porcine plasma.

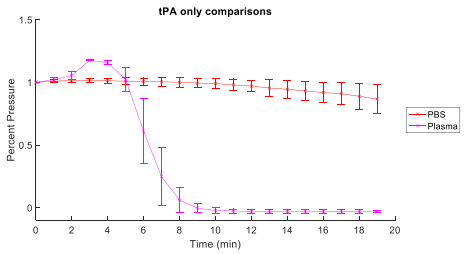

Figure 1. tPA with no ultrasound was tested in both PBS and plasma with the same day clot. It can be seen that tPA in plasma reperfused completely while tPA in PBS only had a slight pressure drop after twenty minutes of treatment.

The reason behind the large difference was hypothesized to be caused the higher concentration of plasminogen in porcine plasma, leading to more plasminogen activated by tPA into plasmin that would cleave the fibrin in the thrombus.

Conclusion

The combination of tPA and inertial cavitation in pig plasma was determined to cause the fastest reperfusion. This indicates that *in vitro* models using PBS instead of plasma or whole blood may underestimate the effects of thrombolytics and US in an *in vivo* model.

Cardiopulmonary Bioengineering: Determining the effects of Varying Porosity of Gas Exchange Fibers on Coagulation in Artificial Lung Devices

Divya Bramharouthu

Introduction

Tens of thousands of patients each year are in desperate need of lung transplants, but are not able to acquire one before it is too late. The odds of survival can be increased if there were an efficient bridge to lung transplantation. Dr. Keith Cook's model for the compliant thoracic artificial lung offers a solution to this problem. The compliant thoracic artificial lung (CTAL) proves to have excellent biocompatibility, provides respiratory support, and greatly decreases blood flow resistance, coagulation, and organ failure. In order to further the biocompatibility of the CTAL device, this research project aims to determine how the rate of coagulation is affected by varying porosities between gas exchange fibers within the device. The experiments consist of *in vivo* testing simplified versions of the artificial lungs encased with 50%, 60%, and 70% porosity gas exchange fibers.

Materials and Methods

Coagulation occurs at the blood-biomaterial interface, being induced by platelet activation through shear stress that increases with increasing surface contact. Utilizing different gas exchange fiber porosities can control the amount of surface contact. Lower porosities correspond to higher packing densities, which lead to an increase in surface area contact for the blood and platelets as they pass through the device. Surface contact and shear stress activates platelets, which cause coagulation. This experiment aims to determine how the varying levels of porosity affect activated clotting time in artificial lung devices.

The project consists of testing three different levels of porosity— 50%, 60%, and 70%. A simplified artificial lung design is used in effort to decrease variability in the experiments. A circuit is designed using medical grade tubing to run these three devices in parallel with a sheep model. Once the resistance of a device doubles, this is an indication of significant clotting and thus, the device is removed from the circuit. The experiment continues until the resistance of the devices double, or a maximum of 4 hours has been reached. Ideally, the device with 50% porosity gas exchange fibers will clot off first, followed by the 60% device, and lastly the 70% device.

Results and Discussion

The *in vivo* trial lasted a total of 30 minutes. The resistances of the devices more than doubled and clotted off in the order of 50% within 15 minutes, 70% in 30 minutes, and lastly 60%. When examining the fibers inside the mini lung, sufficient coagulation was present in the inlets of the devices. The graph below shows the trend of increasing resistance of the devices due to clot formation over time.

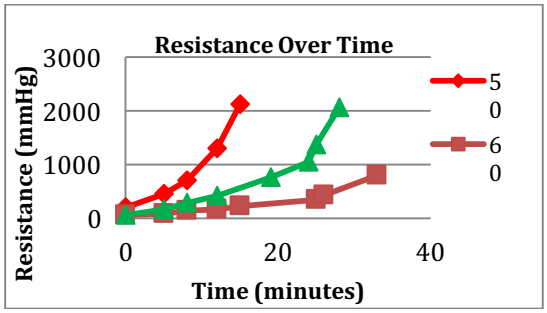

Conclusion

Since the devices clotted off in the order of 50%, 70%, and 60%, instead of the hypothesized order of increasing porosity. This might be due to several factors. One being that the 60% device was in the middle of the three-way connector so possibly had more direct flow. Another factor might be that the 70% had more weaving fiber present than the 60%, which is known to be a site of coagulation. Further studies would include randomizing the order of the devices in the parallel circuit.

Tissue simulating silicone phantom for near-infrared imaging

Yuanyuan Fu
Kainerstorfer Lab

Introduction

Near-infrared spectroscopy (NIRS) is an optical imaging technique that uses light in the near-infrared range to measure hemoglobin concentration in tissue. It is often used for studying angiogenesis of breast cancer. To test the performance of NIRS devices, tissue simulating silicone phantoms are needed and fabrication is the emphasis of this project. The first focus of this research was to fabricate phantoms with optical and mechanical properties of breast tissue and lesion tissue. The second focus was to establish a dynamic phantom with blood mimicking dye that has hemoglobin optical properties to validate NIRS devices in tissue perfusion settings. Tissue simulating phantoms are critical to NIRS studies since they can validate a NIRS device and thus decrease the needs for human subjects. In this research, silicone based phantoms were modeled at 684 nm and 828 nm.

Materials and Methods

A typical phantom is composed of a matrix agent, an absorbing agent and a scattering agent. In this study, the matrix material was silicone. Sorta clear 40, Sorta clear 18 and Ecoflex 0010 (Smooth-On Inc., Macungie, PA) were three types of silicone materials that were used in this research with different degrees of hardness. The absorbing and the scattering agents were India ink and titanium dioxide. To fabricate a phantom, all the reagents were first mixed and degassed using a vacuum degassing chamber. The phantom was then cured in a cylindrical container with an embedded channel. To measure the cured phantom, frequency domain NIRS system (ISS Inc., Champaign, IL) and a non-contact NIRS device were used. The optical properties were calculated using the diffusion equation.

To simulate tissue perfusion in a breast phantom, blood mimicking dye solutions were made. Dye with deoxygenated blood characteristics was a Phosphate Buffered Solution (PBS 1x) based mixture of 0.165% v/v India ink and 2.67% v/v cyan ink. Dye with oxygenated blood characteristics was a PBS based mixture of 0.088% v/v India ink and 0.0098 mg/L Epolight 2735(Epolin Inc., Newark, NJ) [1]. These formulated solutions were flew through a 1 cm deep channel embedded inside the phantom using a peristaltic pump. The absorption coefficient spectrum of the solutions were then measured using the frequency domain NIRS system.

Results and discussion

The optical properties of phantoms that mimic normal breast tissue and breast lesion tissue are summarized in Table 1. Based on literature references, the absorption coefficient(μ_a) of the breast phantom is found to be 3 times higher than of real breast tissue [2]. However, for the purpose of this project, this result is acceptable since NIRS measures change in hemoglobin concentration and thus evaluating change in absorption coefficient is the focus of this study. μ_a for lesion phantom is higher than that of breast phantom because lesion is associated with angiogenesis. The mechanical properties of the phantoms are represented by the Young's modulus of the silicone materials since silicone constitutes the largest proportion of a phantom.

For perfusion simulating phantom experiments, the percentage change of μ_a for oxygenated blood mimicking solution is calculated to be 1% and that of deoxygenated blood mimicking solution is 4%, which are close to the change in hemoglobin absorption observed in tissue perfusion.

Table 1. Phantom optical and mechanical properties

	$\mu_{a\text{ - }684\text{ nm}}$ (cm^{-1})	$\mu_{a\text{ - }828\text{ nm}}$ (cm^{-1})	$\mu_{s\text{ - }684\text{ nm}}$ (cm^{-1})	$\mu_{s\text{ - }828\text{ nm}}$ (cm^{-1})	Young's modulus
Breast phantom	0.1776	0.1824	7.8144	5.6690	10.5 kPa(Ecoflex 0010)
Lesion phantom	0.5172	0.5150	9.2762	7.1950	1.3 MPa(Sorta clear 40)

Conclusions

The results for phantom measurements and dynamic phantom experiments show that the fabricated phantoms highly simulate tissue properties and thus can be used for testing newly developed NIRS systems. For future studies, the stiffness of the phantom should be quantified using a durometer for accurate assessment of mechanical properties. Also, it is suggested to decrease the amount of absorbing agent added to the phantom so that the optical properties of the phantom would be even closer to those of real tissue.

Reference

1. T. J. Akl, R. Long, M. J. McShane, M. N. Ericson, M. A. Wilson, and G. L. Coté. "Optimizing Probe Design for an Implantable Perfusion and Oxygenation Sensor," Biomedical Optics Express. **2**(8), 2096-2109 (2011).
2. P. G. Anderson, J. M. Kainerstorfer, A. Sassaroli, N. Krishnamurthy, M. J. Homer, R. A. Graham, and S. Fantini. "Broadband Optical Mammography: Chromophore Concentration and Hemoglobin Saturation Contrast in Breast Cancer," PLOS ONE **10**(3) (2015).

Using near-infrared spectroscopy to determine the relationship between functional connectivity and cerebral autoregulation and their development with age.

Nin Rebecca Kang
Kainerstorfer Laboratory

Introduction: Using functional near-infrared spectroscopy (fNIRS), hemodynamic signals that contain valuable information about brain activity can be non-invasively measured at very low frequencies ranging from 0.01-0.10 Hz. Of particular interests in my research are the physiological development of functional connectivity and cerebral autoregulation with age as well as the relationship between them. Mapping resting-state functional connectivity (FC) reveals spontaneous brain activity generated under resting conditions (where one sits still and breathes normally), representing specific patterns of synchronous activity. It identifies networks which are consistently found in healthy subjects. fNIRS is capable of mapping FC in the ventromedial prefrontal cortex. On the other hand, cerebral autoregulation (CA) is a mechanism within mammals that maintains an approximately constant flow of blood to the brain despite fluctuations in blood pressure. It is vital to survival as the brain is enclosed in an inflexible skull, so blood flow needs to be relatively constant to maintain optimal intracranial pressure. Both types of brain activity are strong indicators of health in individuals, thus deepening our understanding of them would pave the way for future clinical applications, where they can be used to monitor cerebro-vascular pathologies, brain injuries and overall proper development of children. In recent years, headway has been made to quantify CA and map FC accurately with fNIRS.

The Kainerstorfer laboratory has recently demonstrated that fNIRS can be used to quantify CA using transfer function analysis. Tests on healthy adults have revealed that hyperventilation increases CA efficiency (Kainerstorfer et al 2015). In another study, Eggebrecht et al 2014 developed a high-density diffuse optical tomography (HD-DOT) imaging array that can map higher-order, distributed brain function. This novel fNIRS system has shown that resting state functional connectivity (FC) of the brain can be mapped out with comparable accuracy to fMRI. Other studies have studied both CA and FC thoroughly as separate entities, however, the relationship between the two remains vague. Arivame et al 2015 reported that "…impaired CA was associated with reduced structural and functional connectivity in cerebral networks…", hinting at a connection between CA and FC that has yet to be fully understood. Therefore, with so many areas still to be explored, this study will investigate how CA affects FC in the ventromedial prefrontal cortex, and the development of both over a wide age range.

Materials and Methods: 4 data sets were collected – one from children during free play, and the other three from adults during free play, normal breathing and hyperventilation. A total of 19 children, aged 3 to 12, and 13 adults participated in the experiments. The modified Beer-Lambert law was used to convert intensity of near-infrared light measured in subjects into concentrations of oxy- and deoxyhemoglobin. To map FC, data was filtered using an elliptic filter from 0.01-0.10 Hz. Both Pearson and partial correlation between every pair of channels were calculated for every subject, and partial correlation coefficients were plotted in a correlation matrix for all four data sets for comparisons on FC to be made. Partial correlation was chosen to map FC because it removed the effect of global systemic physiological changes in the brain from the correlation between channels. To quantify CA, data was filtered using a FIR filter at nine frequencies from 0.025-0.0105 Hz to check for phase stability of signals, which determined that the phase difference between oxy- and deoxyhemoglobin should be used to quantify CA because the weak and noisy signals obtained resulted in large error bars, and necessitated large phase differences to be analyzed in order for the figures to be statistically significant.

Results and Discussion: FC mapped for adults during normal breathing and hyperventilation revealed that hyperventilation increased FC locally in channel 3-10. FC maps for adults during normal breathing (resting state) and free play were similar, suggesting free play can be used as a proxy for resting state. Children's data was too noisy to show increased CA, and when FC was plotted against age, there was a very weak linear relationship between the two.

Conclusions: Hyperventilation increased both CA and FC (locally), suggesting a positive relationship or association between them. Much more data from children of the same ages should be collected in order to study the development of CA and FC over a wide age range. This also showed that using spontaneous oscillations produced by the body to quantify CA produced very weak and unstable signals, hence this is not a more robust way of quantifying CA.

Efficacy of Rivaroxaban as an Anticoagulant for Medical Devices

Aakash Parekh
Department of Biomedical Engineering at Carnegie Mellon University

Introduction: Over 12 million Americans are currently suffering from chronic respiratory insufficiency and, for them, current methods for aided ventilation such as extracorporeal membrane oxygenation (ECMO) are thoroughly inadequate. With the supply of lung transplants not nearly meeting demand, artificial means of support are necessary to sustain patients before obtaining a viable donor lung. A major issue with such medical devices is their tendency to activate blood, forming clots. Clotting, or coagulation, decreases the performance and life span of the device. For artificial lungs, the artificial fiber surface activates the intrinsic clotting pathway. For over 50 years, heparin and warfarin have been the only widespread available oral anticoagulants for patients, but entail a host of limitations, such as necessary monitoring, variable pharmacokinetics, and lagged onset and offset. In addition, both are indirect drugs, inhibiting the clotting cascade through interactions with peripheral molecules. Of late, a new wave of direct oral anticoagulants is under research which eliminate many of the downsides of heparin and warfarin and, thus, can be beneficial for eventual home-use. One such drug is rivaroxaban, a Factor Xa inhibitor that prevents conversion of prothrombin to thrombin, thereby preventing fibrin production. This study assesses the anticoagulation efficacy of rivaroxaban through small-scale incubation experiments.

Materials and Methods: For this study, heparin and rivaroxaban were compared at concentrations yielding equivalent activated partial thromboplastin time (aPTT) increases. aPTT is an assay measuring the activity of the intrinsic clotting pathway. Based on prior studies detailing drug concentration versus aPTT for heparin and rivaroxaban, concentrations causing a 1.5x and 2.5x increase from baseline aPTT were selected for each drug. The heparin was diluted in saline and the rivaroxaban was diluted in a 3% DMSO-saline solution. The diluted drugs were added to 2.150 mL of citrated sheep blood to achieve the desired concentrations. A platelet count and activated clotting time (ACT) was performed on the blood for quality control purposes. Two 2.150 mL blood samples were prepared for each drug concentration and incubation time (15 min, 45 min, 90 min), along with a control sample for each incubation time. 0.50” by 0.25” 70% porosity polypropylene fiber bundles were wet in PBS, dried for 10 seconds, and weighed, before being placed in each of the blood samples. The blood samples were then recalcified and incubated for the corresponding durations of time. Following incubation, the samples were each soaked in PBS five times for five minutes each, dried for 10 seconds, and weighed once again. By comparing the average percent increase in weight for the fibers at each incubation time for each drug concentration, a determination can be made of how the anticoagulation effects of rivaroxaban compare to heparin at equivalent relative aPTT levels.

Results and Discussion: Fiber weight percent increases are higher for the lower heparin concentration versus the higher concentration at every incubation time, as expected. Fiber weight percent increases appear to be higher for shorter incubation times and lower for longer times for the lower rivaroxaban concentration versus the higher concentration, however. In addition, for both the 1.5x and 2.5x aPTT increase corresponding concentrations for each drug, rivaroxaban is generally more heavily clotted at every incubation time. The 2.5x aPTT increase rivaroxaban and heparin concentrations for the 15-minute incubation time, however, have comparable clotting. The control fibers’ clot formation was strongly positively correlated with incubation time, as expected.

Conclusions: Rivaroxaban appears to have comparable effects to heparin at higher concentrations and shorter incubation times but seems to clot significantly more at higher incubation times. One possibility of why is if rivaroxaban potentially has effects beyond inhibiting Factor Xa that enhance another aspect of the clotting cascade. Initially the Factor Xa inhibition could be the dominant effect but, over time, the alternate effects gain traction. That could also explain why the higher rivaroxaban concentration creates more clot than the lower concentration at longer incubation times. Upcoming experiments will test varying heparin and rivaroxaban concentrations at a constant 15-minute incubation time to determine what rivaroxaban concentration provides anticoagulation similar to therapeutic heparin doses.

Acknowledgements: CMU Undergraduate Research Organization, CMU Biomedical Engineering Department, Dr. Amy Burkert, Dr. Keith Cook, Rei Ukita